# Conformational Disorder Enhances Electron Transfer Through Alkyl Monolayers: Ferrocene on Conductive Diamond

Rose E. Ruther,[†,‡] Qiang Cui,[†] and Robert J. Hamers*,[†]

[†]Department of Chemistry, University of Wisconsin-Madison, 1101 University Avenue, Madison, Wisconsin 53706, United States

S *Supporting Information*

ABSTRACT: We have investigated the electron-transfer kinetics of ferrocene groups covalently tethered to surfaces of conductive diamond electrodes. Electrochemical measurements show that the rates are only weakly dependent on chain length but are strongly dependent on the surface coverage; these observations are contrary to what is commonly observed for self-assembled monolayers on gold, pointing to important mechanistic differences in electron transfer processes on covalently bonded materials. Molecular dynamics simulations show that dependence on chain length and molecular density can be readily explained in terms of dynamic crowding effects. At low coverage, conformational flexibility of surface-tethered alkyl chains allows the redox-active ferrocene group to dynamically approach the diamond surface, leading to facile electron transfer for all surface molecules. As the coverage is increased, steric crowding causes the average ferrocene-to-surface distance to increase, decreasing the electron transfer rate. Even at the most dense packings, the mismatch between the spacing of surface lattice sites and the optimum alkyl chain density leads to voids and inherent disorder that facilitates electron transfer. These results are significant in the design and optimization of electrocatalytically active surfaces on covalently bonded materials relevant for electro- and photocatalysis.
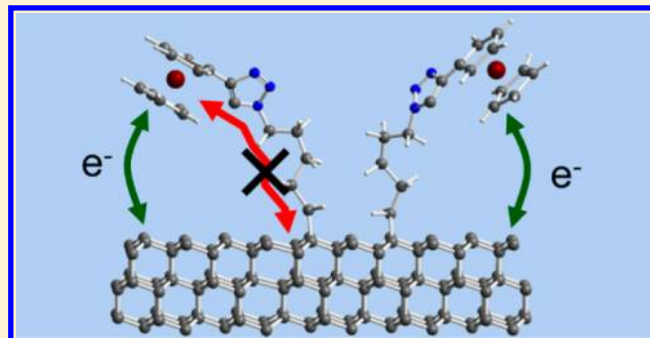
INTRODUCTION

Covalently tethered redox-active molecules are important for many applications in photo- and electro-catalysis,[1−4] sensing,[5,6] and information storage.[7,8] While the vast majority of studies of electron transfer have been performed using self-assembled monolayers (SAMs) on gold,[9−26] covalently bonded materials such as silicon[8,27,28] and TiO_2[3,4,29] are of increasing interest because of their enhanced stability and/or ability to couple light with catalytic reactions. Diamond electrodes have recently emerged as attractive electrode substrates for electrochemistry and electrocatalysis due to their high conductivity, wide potential window, high stability, and low and stable background currents.[30−37] Boron-doped diamond electrodes are highly conductive (<0.1 ohm-cm) and offer improved corrosion resistance compared with sp^2-hybridized forms of carbon such as graphite and glassy carbon.[32−34,37] In recent studies, we showed that redox-active molecular complexes could be covalently attached to the surface of conductive diamond electrodes through alkyl tethers to yield very stable, electro-active surfaces. These redox-active surfaces are able to withstand strongly oxidizing potentials (1.5 V vs the normal hydrogen electrode)[38] and strongly reducing potentials sufficient to achieve catalytic reduction of CO_2,[1] suggesting utility in a broad range of electrocatalytic applications.

A key question in the formation of redox-active surfaces is the electronic nature of the molecular tether linking the electroactive group to the surface. Ferrocene has been widely used as a model system for understanding charge transfer across molecular interfaces to electrodes.[11−13,15,16,22,24−26,37,39−55] Most measurements of electron transfer rates across molecular layers have used self-assembled monolayers on metal surfaces, especially gold[10−26] while fewer studies have investigated electron transfer rates on covalently bonded substrates such as silicon,[46,49,50,52,53,56] conductive oxides,[51] or carbon-based electrodes.[44,48] An important distinction between metallic and nonmetallic substrates is that while on coinage metals adsorbed molecules are able to diffuse laterally to achieve dense, crystalline monolayers, once molecules are bonded onto covalent materials such as silicon and diamond they generally cannot diffuse at room temperature. Furthermore, the distance between adjacent surface sites is not well matched to the optimum 5 Å spacing between ordered alkyl chains.[57−60] Consequently, molecular layers on covalent materials are typically less well-ordered than those on gold. While an understanding of how factors such as molecular chain length, packing, and disorder affect electron transfer in these systems is essential to the optimal design of "smart" molecular interfaces, a fundamental understanding of how these factors influence electron transfer kinetics of covalently bonded monolayers remains poorly understood.

Here, we use ferrocene on boron-doped diamond as a model system to investigate electron-transfer processes through molecular layers covalently bonded to electrode surfaces. Our results show that, contrary to what is typically observed on gold, electron transfer rates are only weakly dependent on molecular length, with fast electron transfer rates achieved even using relatively long alkyl tethers. By measuring the electron transfer rate as a function of alkyl chain length and of the molecular packing density and combining the experiments with molecular dynamics calculations, our results provide important new insights into how the structure and dynamics of the molecular layers on diamond impact their suitability as platforms for electron transfer and catalysis. Our results show the importance of dynamic molecular disorder as a mechanism for enhancing electron-transfer rates and have significant implications for the design of molecular interfaces to covalent materials for applications such as photo- and electro-catalysis.

■ EXPERIMENTAL SECTION

Covalent Attachment of Ferrocene Groups to Boron-doped Diamond Electrodes. Free-standing electrochemistry grade ("EC") boron-doped diamond electrodes having boron concentrations of $>10^{20}$ cm^{-3} and resistivity of 0.02−0.18 ohm-cm (Element VI Corporation) were used for all measurements except atomic force microscopy (AFM) characterization. AFM characterization was carried out using a cleaved natural single crystal of boron-doped diamond obtained on loan from a private source. Ferrocene groups were tethered to the diamond surfaces via photochemical grafting process depicted in Scheme 1, by photochemically grafting an unsaturated

Scheme 1. Covalent Attachment of Ferrocene Groups to H-Terminated Diamond Surface through CuAAC "Click" Reaction[a]
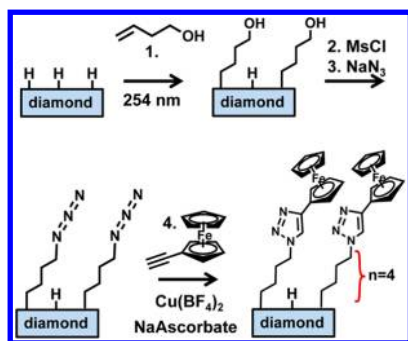
[a]Shown here is the reaction with butenol, leading to a 4-carbon chain. Similar procedures hold for other reactants.

alcohol to the surface and then using the Cu(I)-catalyzed azide−alkyne cycloaddition (CuAAC) "click" reaction to link ethynylferrocene to the surfaces.[29,38]

The following alkenes were used for surface functionalization: 3-buten-1-ol (Sigma Aldrich), 5-hexen-1-ol (Sigma Aldrich), 7-octen-1-ol (TCI), and 11-undecen-1-ol (Sigma Aldrich). Diamond samples were hydrogen terminated prior to use by hydrogen plasma treatment.[61] The hydrogen-terminated diamond samples were covered with a thin layer of the appropriate alkene (previously purged with argon), covered with a fused silica window, and illuminated with ultraviolet light (254 nm, ~10 mW/cm^2) in a sealed cell under an argon atmosphere. Typical illumination times were between 4 and 16 h in order to vary the surface coverage. After reaction the samples were sonicated in isopropanol and dried under N$_2$. To convert the surface alcohol groups into the mesylate, samples were placed in a solution containing 10 mL methylene chloride, 1 mL triethylamine, and 1 mL methane sulfonyl chloride. The samples were reacted for 1 h in an ice

bath. After reaction, the samples were sonicated in methylene chloride and dried under N$_2$. Replacement of the mesylate intermediate with azide was accomplished by treating the samples overnight in a saturated solution of sodium azide in dry DMSO at 80 °C. After reaction with sodium azide the samples were sonicated in water, acetone, and again in water and dried under N$_2$. The CuAAC reaction with ethynyl ferrocene was carried out in a solution of 4 mM ethynyl ferrocene, 2 mM Cu(BF$_4$), and 8 mM sodium ascorbate in a 3:1 (v/v) DMSO/H$_2$O mixture for 3 h. The samples were sonicated in water, acetone, and methylene chloride for 5 min each and stored in isopropanol until further use.

X-ray Photoelectron Spectroscopy (XPS) Measurements. XPS data were obtained using a modified Phys. Electronics system equipped with a monochromatized aluminum K_α source (1486.6 eV), a quartz-crystal X-ray monochromator, and a 16-channel detector array. Spectra were obtained using a takeoff angle of 45°. For quantitative analysis the peaks were fit with Voigt functions after subtracting a Shirley background[62] to compensate for inelastic scattering.

Fourier Transform Infrared Spectroscopy (FTIR) Measurements. Infrared spectra were collected using an FTIR spectrometer (Vertex 70, Bruker Optics) with a liquid nitrogen-cooled HgCdTe detector. FTIR spectra were collected at a resolution of 4 cm^{-1} in single-bounce external reflection mode using a variable angle specular reflectance accessory with a wire grid polarizer (VeeMAX II, Pike Technologies). All reflection spectra were collected with p-polarized light at an incident angle of 50° from the surface normal. FTIR spectra of functionalized surfaces were measured using a clean hydrogen-terminated sample as the background. Residual sloping baselines were removed to improve the clarity of the spectra.

Atomic Force Microscopy Measurements. AFM measurements were taken with a Veeco Nanoscope IVa instrument. Tapping mode diamond-like-carbon coated tips (Tap300Al-G-DLC, Budget Sensors) were used for both imaging and scratching. The scratching was carried out in contact mode and tapping mode was used to image a larger area than the scratched rectangle.

Electrochemical Characterization. Electrochemical measurements were performed using an Autolab potentiostat (PGSTAT302N, Metrohm Autolab B.V.) and a three-electrode cell. The diamond samples were used as the working electrode with an exposed area of 0.275 cm^2, and a platinum wire was used as the counter-electrode. The reference electrode was Ag/AgCl/3 M NaCl (BASi). All potentials are reported with respect to this reference. HClO$_4$ (1 M) was used as the electrolyte. Impedance spectroscopy measurements used a 10 mV RMS amplitude modulation. Nova software (Metrohm) was used to fit impedance data to circuit models.

Molecular Dynamics Simulations. The force-field parameters used to describe the aliphatic chain and the diamond surface were based on similar atom types from the CHARMM22 force field.[63] As a simplification, the triazole linkage was replaced by an imidazole and the ferrocene moiety was represented by a Lennard-Jones sphere. Since the main effect is likely due to the steric repulsion between neighboring aliphatic chains, these simplifications are expected to be appropriate for our purpose. The Lennard-Jones sphere that models ethynylferrocene was described with a radius of 3 Å and a very shallow well-depth of 0.001 kcal/mol. The molecular dynamics simulations were carried out using CHARMM.[64] To approximately describe the impact of water on the chain dynamics, Langevin dynamics[65] were used at 300 K with a friction constant of 25 ps^{-1} for non-hydrogen atoms; this protocol is widely used in biomolecular simulations in which the solvent molecules are treated implicitly.[65,66] Considering the largely nonpolar nature of the grafted chains and of the diamond surface, ignoring the explicit solvent and counterions is likely to have a very minor impact on the equilibrium conformational distributions of the grafted chains, which are the quantities of interest. All bonds including hydrogen were constrained using SHAKE,[67] and the integration time step was 2 fs except for the high-coverage case (24 chains), for which a time step of 1 fs was used. The diamond atoms were held fixed during the simulations. For each model system, two independent sets of simulations were carried out; the length of the

simulations ranged from 5 to 10 ns. Snapshots were obtained using the program Virtual Molecular Dynamics (VMD).[68]

■ RESULTS

AFM "scratching" methods[69] were used to investigate the structure of the photochemically grafted layers. Because for this measurement the sample needs to extremely flat, we used a natural single crystal of boron-doped diamond that was cleaved along the (111) crystal plane. The cleaved diamond was H-terminated and then grafted for 16 h with undecenol. The sample was imaged in tapping mode, and a smaller region was scanned in contact mode with a larger force. The sample was then reimaged in tapping mode. Figure 1 shows the resulting
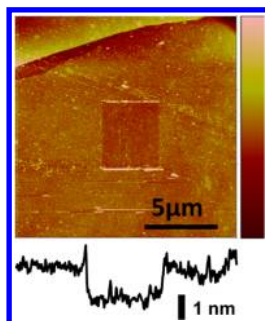

Figure 1. AFM image of cleaved single crystal diamond grafted with undecenol for 16 h. The center rectangle is where the undecenol has been removed by the AFM tip. The color scale spans a range of 20 nm. The lower trace shows the height contour measured from left to right across the scratched region.

AFM image, with the central "scratched" region clearly visible. The height profile shows that in the scratched region the surface height is 1.3 nm lower than the surrounding regions, thereby indicating that the molecular layer is 1.3 nm in height. This value is very similar to that reported for SAMs on gold formed from thiols with alkyl chains of similar length to undecenol[22] and is consistent with the expected length of 1.5 nm. The AFM data show that the photochemical grafting procedures used here yield high-quality, uniform molecular layers with no evidence for multilayer formation even at the longest grafting times.

Characterization of Surface Functionalization. Successful covalent attachment of ferrocene groups to the diamond surface via the CuAAC reaction was established using FTIR, XPS, and cyclic voltammetry measurements. Figure 2a shows FTIR spectra of an azide terminated diamond sample before and after reaction with ethynyl ferrocene. The data shown are for a sample that was initially reacted with 3-buten-1-ol for 16 h; similar results (not shown) were obtained with the longer chain alcohols. The stretch at 2090 cm^{-1} is characteristic of the asymmetric stretch of the azide group.[37] This stretch disappears after reaction with ethynyl ferrocene, consistent with reaction of the azide group with the alkyne.

Figure 2c shows Fe(2p) spectra of the sample exposed to the full CuAAC reaction condition; the spectrum shows sharp peaks at 708 and 720 eV characteristic of ferrocene with iron in the 2+ oxidation state. Also shown is the alcohol-terminated sample after exposure to ethynyl ferrocene. This control sample shows only broad, weak peaks near 711 and 725 eV. Some small intensity at these energies can also be observed on the full CuAAC sample. The 711 and 725 eV peaks are characteristic of ferrocenium where the iron is in the 3+ oxidation state.[45,50] The
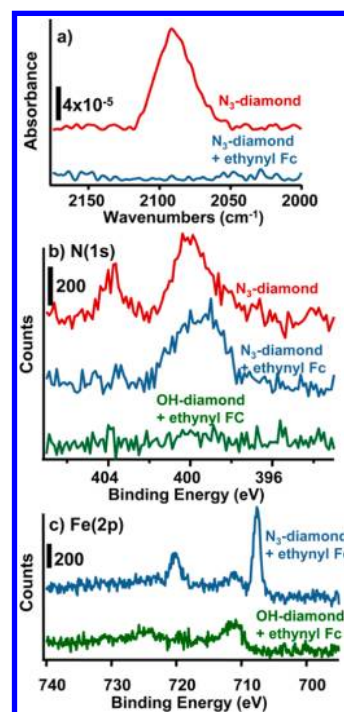
Figure 2. Characterization of successful CuAAC reaction of ferrocene with N$_3$-modified diamond before and after exposure to ethynyl ferrocene. (a) FTIR spectra showing the disappearance of the 2090 cm^{-1} azide stretch upon exposure to ethynylferrocene. (b,c) XPS of azide terminated diamond before and after reaction with ethynyl ferrocene. Also shown are results from a control sample, consisting of the alcohol-terminated surface that was exposed to ethynyl ferrocene under the CuAAC reaction conditions.

presence of Fe in this oxidation state may be induced by charging and/or by the incident X-rays. The XPS results show that ferrocene is specifically bound to the surface through the CuAAC reaction.

Figures 2b and 2c show N(1s) and Fe(2p) XPS data, respectively, of azide-modified diamond before and after exposure to ethynylferrocene. To rule out the contribution of physisorbed ferrocene molecules, results are also shown from control experiments in which the intermediate alcohol-terminated diamond surface was exposed to ethynyl ferrocene under identical reaction conditions. The N(1s) signal of the azide-modified diamond shows a characteristic set of two peaks at 405 and 400 eV in approximately a 1:2 intensity ratio.[13] The peak near 404 eV is characteristic of the azide group and arises from the electron-deficient central N atom of the $-N \equiv N^+ \equiv N^-$ resonance structure. After the CuAAC reaction the 404 eV peak disappears and the N(1s) spectrum shows only a single broad peak near 400 eV, consistent with the conversion of the azide group into the triazole ring. As expected, the alcohol-terminated sample shows no N(1s) intensity, establishing that the N(1s) observed in the other samples arises solely from the grafted azide groups and their subsequent triazole ring.

Quantitative analysis of the XPS Fe and C peak areas and using the equation $N = (A_{Fe}/A_C)(S_C/S_{Fe})\rho_C \lambda_C$ where N is the area density of Fe atoms, A_{Fe} and A_C are the area of Fe(2p) and C(1s) features, S_{Fe} and S_C are the respective atomic sensitivity factors, ρ_C is the atomic density of diamond (1.7×10^{23} atoms/cm^3),[70] and λ_C is the inelastic mean free path of C(1s) electrons in diamond (=1.8 nm)[71] yielded an estimated coverage of $N = 1.3 \times 10^{14}$ Fe atoms/cm^2. This equation assumes that the C(1s)

signal comes from the diamond substrate. Previous studies estimated the theoretical maximum coverage of ferrocene groups to be 2.65×10^{14} cm^{-2} based on a close-packed layer of spheres with 6.6 Å diameter;[12] an experimental maximum coverage of 2.6×10^{14} was reported previously for monolayers of ferrocene-terminated alkanethiols on gold.[13] Random packing (as might be expected on a covalent surface) of 6.6 Å diameter spheres would yield a slightly lower coverage of 2.4×10^{14} molecules/cm^2.[72] The maximum coverage we measured is less than this, even for samples that have been illuminated for long times (16 h) in the initial photochemical grafting step.

Electrochemical Characterization via Cyclic Voltammetry. To determine whether the ferrocenium is electrochemically active, cyclic voltammograms (CVs) were obtained. Figure 3 shows CVs of the full CuAAC sample and the control sample consisting of the alcohol-terminated surface that was exposed to ethynylferrocene.
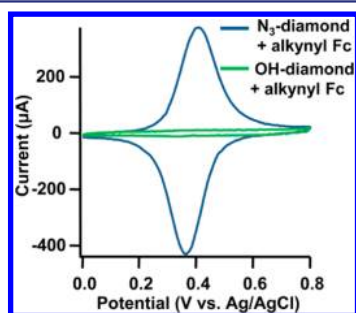
Figure 3. Voltammograms (10 V/s) after the CUAAC click reaction. The blue trace shows the azide-terminated surface after reaction with ethynyl ferrocene (Fc). The green trace is a control sample of the alcohol-terminated surface (i.e., no azide) after undergoing the identical reaction conditions with ethynyl ferrocene.

Clear oxidation and reduction peaks are observed for the full CuAAC sample, with $E° = 0.39$ V. The control sample shows no evidence of oxidation or reduction peaks and shows only a small, nearly constant separation between forward and reverse sweeps that is due to the interfacial capacitance. While our XPS data reveal trace amounts of Fe on the control sample, the electrochemistry data show no evidence for electrochemically active iron; this suggests that any physisorbed ferrocenium observed in the XPS is removed from the surface under the CV conditions and not detectable thereafter. The coverage of electrochemically active ferrocene was calculated by integrating the peak areas, yielding 1.6×10^{14} ferrocenes/cm^2, in excellent agreement with the XPS results.

Figure 4 shows cyclic voltammograms obtained at different scan rates for ferrocene groups attached to the diamond surface. The data shown are for a sample that was initially reacted with 3-buten-1-ol for 16 h, with similar results obtained for the longer chain alcohols. The formal potential of 0.39 V vs Ag/AgCl measured from these curves is similar to values reported for other types of electrodes modified with ferrocene through similar chemistry[46,73,74] and is slightly higher than that reported for unmodified ferrocene in solution (~0.2 V vs Ag/AgCl).[75] Prior studies have noted that the triazole ring formed by the CuAAC reaction is an electron-withdrawing group and is expected to shift the formal potential toward more oxidizing potentials.[76,77] The shift toward higher potentials may also be partly explained by the nonpolar monolayer destabilizing the ferrocenium (Fe^{3+}) with respect to the ferrocene (Fe^{2+}).[78]
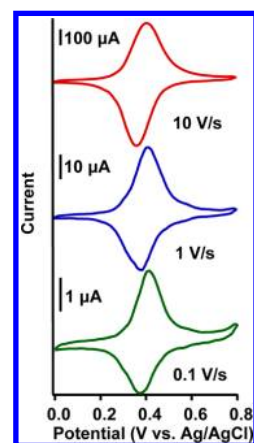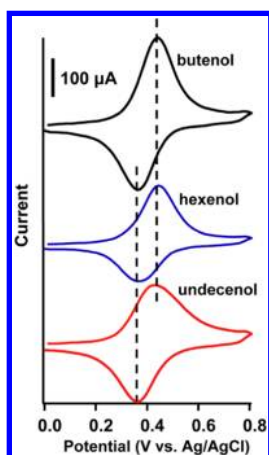

Figure 4. Cyclic voltammograms of diamond electrodes after reaction with ferrocene, measured at different scan rates.

The peak half-width ΔE_{fwhm} is ideally 91 mV for a one-electron transfer at 25 °C.[16,79] Our experiments yield values larger than this, ranging from 120 mV at 0.1 V/s to 150 mV at 10 V/s for the anodic peak. The increased width is similar to that reported previously and has been attributed to the presence of different local environments of the redox couple.[16] The splitting between the oxidation and reduction wave peaks ΔE_{p} is ~40 mV and is independent of scan rate between 0.1 and 10 V/s. While ideally ΔE_{p} is zero in the limit of low scan rates, prior reports have frequently observed nonzero limiting ΔE_{p} and attributed it to changes in the solvation of the redox centers or structure of the monolayer with changing oxidation state.[16] Since ferrocenium is known to specifically ion pair with perchlorate anions,[78] this explanation appears appropriate here. At higher scan rates, the peak splitting is expected to increase as the scan rate becomes comparable to or greater than the electron transfer rate. Since we observe that ΔE_{p} is independent of scan rate for the scan rates used here, our results indicates that the electron transfer rate is fast relative to the CV scan rates used here.

Interestingly, our data show almost no correlation between peak splitting and the length of the alkene used in the initial photochemical grafting step. Figure 5 shows cyclic voltammograms taken at 10 V/s for ferrocene tethered to diamond using different alkyl chain lengths. ΔE_{p} is 70−80 mV independent of chain length for the CVs shown. This suggests that the electron transfer rate is not significantly slowed by longer chains, at least for scan rates up to 10 V/s.

Impedance Analysis of Standard Electron Transfer Rates $k°$. Since the electron transfer rates are too fast to measure accurately via cyclic voltammetry, we performed a more detailed analysis of electron transfer rates using electrochemical impedance spectroscopy. The equivalent circuit for redox couples strongly adsorbed to an electrode surface has been given by Laviron[80] (Figure 6a). It includes the solution resistance, R_{S}, and the double-layer capacitance, C_{DL}. The redox couple contributes an additional charge transfer resistance, R_{CT}, and pseudocapacitance, C_{A}. The solution resistance is in series with the other circuit elements and can be subtracted to yield the simpler Debye equivalent circuit[20,81] (Figure 6b). The Debye circuit has a single relaxation time constant, τ, that is inversely related to the standard electron transfer rate, $k°$:[20,21,82,83]

$$\tau = R_{\text{CT}} C_{\text{A}} = (2k°)^{-1}$$

Figure 5. Cyclic voltammograms of ferrocene tethered to diamond with alkyl chains of different lengths. All scan rates were 10 V/s. Top trace (black) is for an initial photochemical grafting step with butenol. Middle trace (blue) used hexenol and bottom trace (red) used undecenol. All photochemical reaction times were 16 h. Dashed lines are to facilitate visual comparison of peak locations.
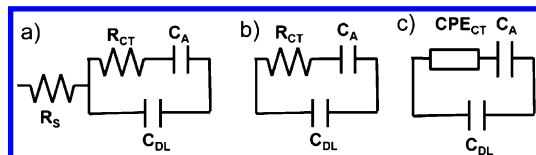
Figure 6. (a) Laviron's equivalent circuit for a redox couple strongly adsorbed to an electrode surface. R_S is the solution resistance and C_{DL} is the double layer capacitance. R_{CT} and C_A are the charge transfer resistance and pseudocapacitance. (b) Debye equivalent circuit. (c) Cole−Cole equivalent circuit.

The Debye circuit yields a perfect semicircle in a Nyquist plot of the dielectric constant with the center of the circle positioned along the real axis.

The dielectric constant, ε, is then given by: $\varepsilon = (j\omega Z)^{-1}$ where j is the imaginary unit, ω is the angular frequency, and Z is the impedance. The magnitude of the imaginary component of the dielectric constant reaches a maximum at a frequency $\omega°$ that is inversely related to the relaxation time constant of the system: $\omega° = \tau^{-1}$. Often systems display a distribution of time constants, rather than a single relaxation time constant.[23,24,84] This is commonly modeled by the Cole−Cole circuit where R_{CT}, a pure resistor, is replaced with a constant phase element (Figure 6c).[20,21,81,84,85] The impedance of a constant phase element (CPE) is given by

$$Z_{CPE} = A(j\omega)^{-\alpha}$$

where A and α are adjustable parameters. The CPE is a simple distributed circuit element that is often used to model frequency-dependent effects that arise from microscopic inhomogeneity or roughness of electrodes.[86]

The Cole−Cole circuit (Figure 6c) also yields a single, circular arc in a Nyquist plot of the dielectric constant, but the center of the circle lies below the real axis.

To determine the standard electron transfer rates, we prepared ferrocene-terminated monolayers with butyl, hexyl, and undecyl chains. For each length, we also varied the ferrocene coverage by changing the duration of the initial illumination step used to link the appropriate alcohol to the surface (step 1, Scheme 1). Times between 4 and 16 h were

used, with the shorter illumination times yielding sparser, submonolayer coverage and the longest times yielding full coverage. For each sample, the final coverage of electrically active ferrocene groups was measured by integrating the peak areas in the cyclic voltammograms. We measured the redox potential of the surface bound ferrocene groups, $E°$, using cyclic voltammetry for each sample and collected impedance data at $E°$ ($\sim$0.39 V vs Ag/AgCl). The solution resistance was measured by taking impedance data at 0.8 V vs Ag/AgCl, a potential far from the redox potential of the ferrocene where the diamond electrode behaves as a simple blocking electrode (solution resistance in series with a double-layer capacitance). The solution resistance was subtracted from the impedance data taken at $E°$ and the data were displayed as Cole−Cole plots (Nyquist plots of the dielectric constant).

Figure 7a shows typical Cole−Cole plots for ferrocene tethered to diamond electrodes using three different alkyl chain
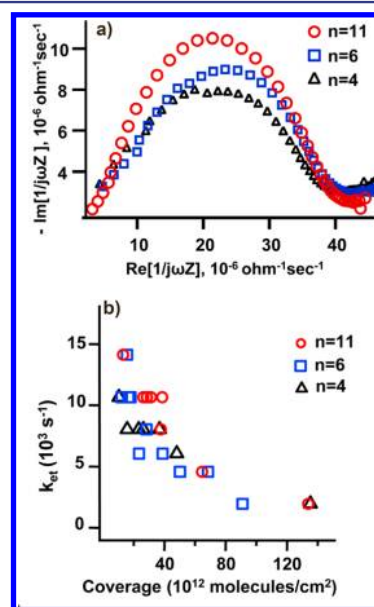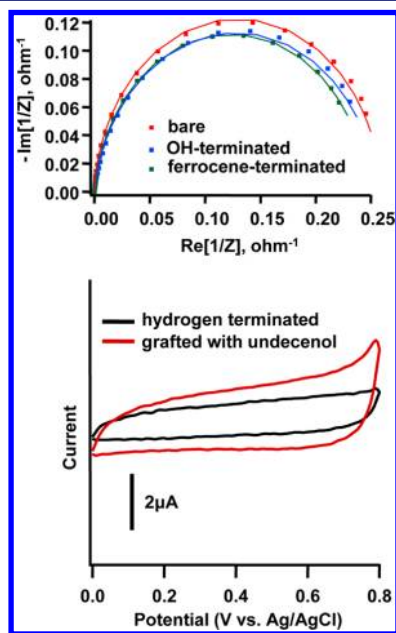

Figure 7. Influence of chain length on electron-transfer rate. (a) Cole−Cole plots for ferrocene tethered to the diamond surface through different alkyl chain lengths. Data were collected at frequencies between 1 and 100 000 Hz. (b) Standard electron transfer rates as a function of ferrocene coverage for different alkyl chain lengths.

lengths, over the frequency range 1 Hz - 100 kHz. We analyzed these data and additional coverage-dependent data using several approaches. Fitting the data with the Cole−Cole circuit shown in Figure 6c yielded excellent results. We also evaluated fits in which the double-layer capacitor C_{DL} was replaced with a CPE; because the differences were small we used the pure capacitance C_{DL} in subsequent analyses. We also found that electron transfer rates obtained directly from the frequency corresponding to the maxima in the Cole−Cole plots (as described above) accurately reproduced the values obtained through more detailed fitting to circuit models. We therefore used this more direct approach for the numerical values reported here.

Figure 7b shows the resulting electron transfer rates k_{et} as a function of ferrocene coverage for three different alkyl chain lengths. For each chain length the electron transfer rate is reasonably high ($\sim$$10^3$−$10^4$ s^{-1}) at low coverage, but decreases as the coverage increases. Surprisingly, there is no significant

difference in electron transfer rate between the molecules with different chain lengths. This is contrary to what has typically been observed for self-assembled monolayers on gold, where longer chain lengths had significantly lower electron transfer rates. We have also measured the half-wave potential $E_{1/2}$ (defined as the average of the potentials corresponding to the peak cathodic and peak anodic currents) and find that there is a small (<0.040 V) increase as the coverage increases. The increase implies that the thermodynamic environment around the ferricenium ion becomes slightly more hydrophobic at higher coverages.[78,87] These data are shown in the Supporting Information.

Measurements of Interfacial Capacitance and Monolayer Structure. To gain insight into the monolayer structure, the double-layer capacitance of a bare, hydrogen-terminated diamond electrode was compared to the capacitance of electrodes after functionalization with undecenol and subsequent modification with ferrocene. The double-layer capacitance was measured by impedance spectroscopy at 0.0 and 0.8 V vs Ag/AgCl, potentials far from $E°_{ferrocene}$ to avoid contributions from the charge-transfer pseudocapacitance in the sample functionalized with ferrocene groups. Figure 8a

Figure 8. (a) Nyquist plots of the admittance for a bare, hydrogen-terminated diamond electrode (red), a diamond electrode after photochemical grafting with undecenol (blue), and a diamond electrode functionalized with ferrocene (green). All data were collected at 0.8 V vs Ag/AgCl. Markers are experimental data. Lines are for best fits to a series R-CPE circuit. (b) Cyclic voltammograms of a bare, hydrogen-terminated diamond electrode and a diamond electrode grafted with undecenol for 16 h. Scan rate 1 V/s.

shows Nyquist plots of the admittance at 0.8 V for a bare, hydrogen-terminated diamond electrode, a diamond electrode grafted with undecenol for 16 h, and a diamond electrode after functionalization with ferrocene groups.

The impedance data were modeled by series R-CPE circuits, where R is the solution resistance (typically ~4 Ω) and the CPE represents the double-layer capacitance.[88,89] Table 1 shows values for the CPE parameters for all three surfaces. All parameters at each voltage are the same within the error of the fits, with the exception of a ~ 40% increase in A after grafting

Table 1. CPE Parameters for the Interfacial Capacitance Derived from Fits to Impedance Data

	0.0 V		0.8 V	
	A (10^{-6})	a	A (10^{-6})	a
bare, H-terminated	1.90	0.96	3.86	0.96
grafted with undecenol	1.74	0.94	5.33	0.92
ferrocene terminated	1.84	0.93	3.88	0.94

*Units of A are $ohm^{-1}sec^{-\alpha}$

with undecenol compared to the bare surface. All α parameters are very close to 1 which is characteristic of a smooth surface. In this case the prefactor (A) is closely related to the interfacial capacitance C, $A \approx C$.
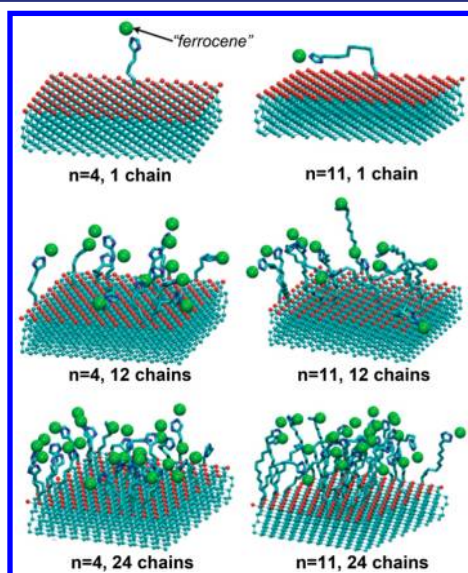
We also confirmed these results using cyclic voltammetry, where in the absence of faradaic processes the only current that flows is that required to charge the double-layer.[35,90] Figure 8b shows cyclic voltammograms at a scan rate of 1 V/s using a bare, hydrogen-terminated diamond electrode and a diamond electrode grafted with undecenol. Again, the vertical separation between forward and reverse sweeps is ~40% larger on the undecenol-modified surface. This shows that grafting with undecenol increases the interfacial capacitance, consistent with the impedance data.

In Figure 8, both cyclic voltammetry and impedance measurements indicate that grafting with undecenol gives rise to a small increase in the interfacial capacitance. This is in contrast to prior measurements for densely packed, self-assembled monolayers on gold, where functionalization with molecular layers typically leads to a pronounced (~50-fold) decrease in the capacitance.[16,22] However, on gold the change in interfacial capacitance is highly dependent on the degree of structural order, as SAMs having more defects and higher ion permeability show much smaller changes in capacitance.[91] Our impedance and CV data on diamond are consistent with the hypothesis that the molecular layers formed on diamond have an intrinsically high degree of structural disorder that allows water and ions to penetrate through the molecular layers. The small increase in capacitance after functionalization likely arises from the fact that the H-terminated diamond surface is very hydrophobic; hence, functionalization with a hydrophilic molecule likely alters the structure of the water and may enhance the local ion concentration near the interface.

Molecular Dynamics Simulations. The rate of electron transfer between the surface and the redox center will depend on the path of electron tunneling, which is highly sensitive to monolayer order and packing.[16] While a through-bond tunneling mechanism has been shown to dominate for long chain alkanethiol self-assembled monolayers,[17] through-space tunneling has been observed for other types of monolayer systems, especially shorter chain lengths.[16,92] To help determine how the surface coverage impacts chain flexibility and the average distance from the ferrocene to the surface, we carried out molecular dynamics simulations using a set of simplified models. Each model includes a specific number of aliphatic chains grafted onto a (111) diamond surface; the surface is approximately 30 Å × 30 Å, with the standard periodic boundary condition applied to all three dimensions; the size of the box in the z dimension is 40 Å. For each aliphatic chain, four levels of coverage were studied, which include 1, 3, 12, and 24 chains, respectively, randomly distributed on the diamond surface; these correspond to a coverage of 0.11, 0.33, 1.33, and 2.77 × 10^{14} molecules per cm^2, respectively. Figure 9

shows representative snapshots for different chain lengths and coverage. Short movies depicting the actual dynamics are included as Supporting Information.

Figure 9. Snapshots of MD simulations using butyl ($n = 4$, left column) and undecyl ($n = 11$, right column) chains, and surface coverage. One, 12, and 24 molecules per slab correspond to coverage of 0.11, 1.3, and 2.7×10^{14} molecules/cm^2. The molecular chain and triazole linkage are shown explicitly; to simplify the depiction, the ferrocene group is shown as a green sphere. Red atoms are the diamond surface atoms.

At short chain lengths and low coverage, the MD simulations show that the ferrocene moiety is closer (on average) to the surface compared with results using longer chain lengths or higher coverage. Distances were measured every picosecond during the production run to obtain the normalized distance distribution $P(z)$. Figure 10a shows the normalized distance distribution $P(z)$ for $n = 4$ (butyl) linkages, using 1 ns simulation times. Also shown is one set of data obtained from a longer (10 ns) simulation time; it shows a distribution nearly identical to that of the 1 ns simulation, demonstrating that the 1 ns simulations have run for a sufficiently long time to capture the correct distance distributions.
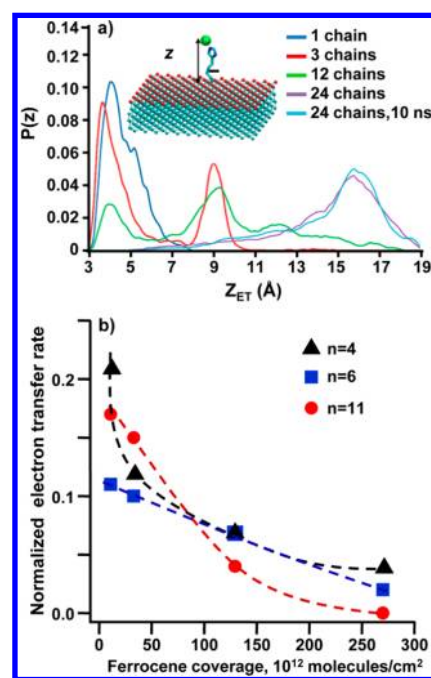
The distribution in Figure 10a shows peaks near 4, 9, and 16 Å depending on coverage. At the lowest coverage the molecules are frequently bent in a configuration that places the ferrocene group very close (~4 Å) away from the surface; as the coverage increases the distribution shifts toward larger distances. The coverage-dependent changes in $P(z)$ are a clear manifestation of the steric repulsion between neighboring chains, which causes the molecule to extend as fully as possible as the coverage increases.

To estimate how these changes affect the effective electron transfer rate (k_{eff}), we integrated the distance distribution with an exponential dependence of the electron transfer rate on the distance from the diamond surface:

$$k_{eff} = \int dz P(z) k(z) = \int dz P(z) k(z_{ref}) \exp[-\beta(z - z_{ref})]$$

where the reference distance z_{ref} was taken to be 3 Å (the radius of the ferrocene[12]) and β is the tunneling parameter.

Figure 10b shows the relative electron transfer rates that were calculated from simulations using different chain lengths and

Figure 10. (a) Probability distribution $P(z)$ for ferrocene groups tethered via butyl chain ($n = 4$) at different molecular coverages. (b) Predicted electron-transfer rates for alkyl chains of different length as a function of coverage. Compare with experimental data in Figure 7b.

coverage. While the current model is too simple to allow quantitative comparison with experimental data, qualitatively good agreement between the experimental values (Figure 7b) and the theoretical predictions (Figure 10b) is obtained with a tunneling parameter $\beta = 1.5$ Å^{-1}. This is consistent with the experimental β value of 1.5–1.8 Å^{-1} estimated for tunneling through water[93,94] and slightly larger than the β value of ~0.85–1.0 Å^{-1} typically measured for self-assembled monolayers where through-bond tunneling dominates the electron-transfer process.[16,17,43]

■ DISCUSSION

The above results demonstrate that ferrocene-terminated monolayers on boron-doped diamond exhibit facile electron transfer,[1,38] but also show several surprising results. First, we observe that the standard electron transfer rates on diamond are nearly independent of molecular length. Second, the electron transfer rates decrease significantly as the coverage increases. Finally, functionalization of the surface increases the interfacial capacitance.

These three observations are quite distinct from what has been observed previously for self-assembled monolayers on gold,[16–19,23,95] where electron transfer rates decrease exponentially with increasing chain length chain length,[16–18,23,26,40] exhibit electron transfer rates that increase at higher coverage,[12] and show pronounced decreases in interfacial capacitance upon functionalization with molecular layers. Our results suggest that the differences in behavior on diamond compared with gold arise from intrinsic differences in the structural perfection within the layers, and particularly, the role that conformational disorder plays in facilitating interfacial electron transfer.[18,23]

We first summarize the most important features of SAMs on gold surfaces, as a point of comparison for our monolayers on diamond. Previous studies of alkanethiols on gold have shown that alkyl chains of adsorbed monolayers are able to form

dense, crystalline layers with nearly close-packing of the alkyl chain; this close-packing is facilitated by the fact that the optimal alkyl chain spacing of 5.0 Å is almost exactly $\sqrt{3}$ times the 2.884 Å spacing between atoms on Au(111), allowing the thiol S atoms to bind to next-nearest neighbor Au atoms on Au(111) and form an ordered $(\sqrt{3} \times \sqrt{3})R30°$ commensurate overlayer.[57−60] Corresponding experiments on layers terminated with redox-active groups have found that in these densely packed systems the electron transfer rate varies with the length of the alkyl chain according to

$$k_{app}^{\circ} = k^{\circ}\exp(-\beta d)$$

where k_{app}° is the apparent standard rate constant for electron transfer, β is the tunneling parameter, and d is the length of the alkyl chain separating the redox-active group from the gold surface.[17,18,24−26,42,43,55,91,95,96] The tunneling parameter β is typically between 0.85 and 1.1 Å^{-1},[97,98] resulting in a very strong decrease in electron transfer rate with increasing length of the molecular tether. Because of the strongly blocking nature of the layer, the electron transfer rates can be strongly affected by defects and, at high coverage the electron transfer rate increases because electrons can transfer between adjacent ferrocene groups and finally transfer via defects or domain boundaries within the monolayer, instead of through-bond tunneling.[99] Compared with the bare gold surface, the introduction of an alkanethiol SAM leads to a decrease in capacitance by introducing a new series capacitance given by $C = (\kappa\varepsilon_0 A/t)$ where κ is the dielectric constant, ε_0 is the permittivity of free space, A is the electrode area, and t is the thickness of the molecular layer.[22] Since the molecular capacitance C_m is in series with and is small compared with the double-layer capacitance C_{DL} (typically ∼15 μF for 1 cm^2 area), the net interfacial capacitance deceases when a SAM is formed on gold.

Our Results Show that a Very Different Picture Emerges on Diamond Surfaces. When organic monolayers form on covalently bonded materials such as diamond, the lattice sites to which the molecules attach are, in general, not well matched to the optimum 5.0 Å spacing between alkyl chains;[58,60] this mismatch leads to a comparatively disordered, less dense distribution of molecules on the surface. At low coverage the attached molecules are highly flexible for all chain lengths, allowing the terminal ferrocene groups to transiently approach the surface and undergo electron transfer. Our experimental data and molecular dynamics simulations show that as the surface coverage is increased, steric crowding reduces the ability of the ferrocene groups to come close to the surface, and the electron transfer rate (per molecule) decreases. The half-wave potential $E_{1/2}$ also increases slightly (∼40 mV), consistent with the expectation that the more hydrophobic environment of the sterically crowded ferrocene groups decreases the thermodynamic stability of the ferrocenium ion and shifts $E_{1/2}$ to more positive values.[87] However, even at the highest attainable coverage the molecular layers are not effective at blocking electron transfer, and our capacitance measurements show a slightly increased capacitance compared with the bare surface.

Bocian and co-workers[49,100] previously reported electron transfer rates for porphyrins tethered to gold surfaces via short, conjugated tethers in nonaqueous electrolytes and observed electron transfer rates that decreased with increasing coverage. They attributed these changes to space-charge effects associated with coverage-dependent changes in counterion motion.[100] Due to the pronounced differences in the tethered molecules

and other experimental conditions it is not possible to provide a meaningful mechanistic comparison of their results with ours, but it is noteworthy that the fastest rates they measured with conjugated linkers are no more than 10-fold faster than what we measure using undecenol, an 11-carbon fully saturated tether.

We postulate the bonding of molecular layers to fixed lattice sites of diamond and the absence of significant lateral diffusion of molecules (due to the strong interfacial C−C bond compared with the much weaker Au−S bond) leads to an inherently high level of disorder within the molecular layers, and that as the coverage increases steric crowding forces the monolayers to become more extended and ordered. To demonstrate this, we simulated (see Supporting Information) the random bonding of 5.0 Å diameter particles (the optimum diameter of alkyl chains) onto the fixed lattice points of a diamond(111) lattice (nearest-neighbor distance = 2.67 Å) and found a maximum packing density of 3.7×10^{14} molecules/cm^2, compared with 4.2×10^{14} molecules/cm^2 expected for randomly packed spheres on a flat surface and 4.6×10^{14} molecules/cm^2 for close-packed spheres.[72] These results show that at least ∼20% void fraction is expected when molecular layers bond to diamond, even at the densest accessible packing. Our results indicate that this significant internal void space provides sufficient conformational flexibility to achieve standard electron transfer of at least ∼10^3 s^{-1}.

The practical importance of the above is that it leads to an understanding of how to design molecular tethers that will enable redox-active molecules such as electro- or photo-catalysts to be integrated onto electrode surfaces. The standard electron transfer rates we measure are $10^3−10^4$ s^{-1}; these values are comparable to or possibly faster than those observed for ferrocene SAMs on gold, where rates on the order of $10^6 − 10^3$ s^{-1} have been reported for molecular layers containing 5−10 methylene groups in the aliphatic chain.[26,43,101] Prior studies have shown that the electron transfer rate between ferrocene in solution and bare gold electrodes is 1−2 orders of magnitude higher than what has been measured at diamond electrodes.[32,102] This difference can been attributed to a lower density of states in boron-doped diamond relative to gold.[103] While this might suggest that the electron transfer rates on diamond are likely to be intrinsically slower than those on gold, prior studies have shown that at the high boron concentrations used here (>10^{20} cm^{-1}) the Fermi level becomes degenerate with the valence band, so that the diamond becomes metallic with a correspondingly high density of states.[104] This metallic character is consistent with the fact that the rates we measure are 2−4 orders of magnitude faster than electron transfer rates typically measured on other carbon-based electrodes.[44,48] Of even greater importance is that the standard electron transfer rates of $10^3−10^4$ s^{-1} we obtain on highly boron-doped diamond films are considerably faster than the turnover frequency of many catalysts of interest.[105−108]

We also emphasize that the dynamic nature of the molecular disorder may be important, as a disordered but structurally rigid layer would likely yield fast electron transfer for a subset of molecules but much slower electron transfer for others. In contrast, the agreement between XPS and electrical measurements of total ferrocene coverage and the well-defined electrochemical rate measurements indicate that nearly all surface-tethered molecules are electrically active and can achieve charge transfer on the scale of ∼10^{-4} second.

For applications such as electrocatalysis, the "best" choice of conditions is likely to be that which maximizes the product of

the electron transfer rate k_{et} and the surface coverage N (number of electroactive groups per unit area) as this product Nk_{et} yields rate of electron transfer per unit area of the sample. Using the data from Figure 7b, Figure 11 shows the results of such an analysis.
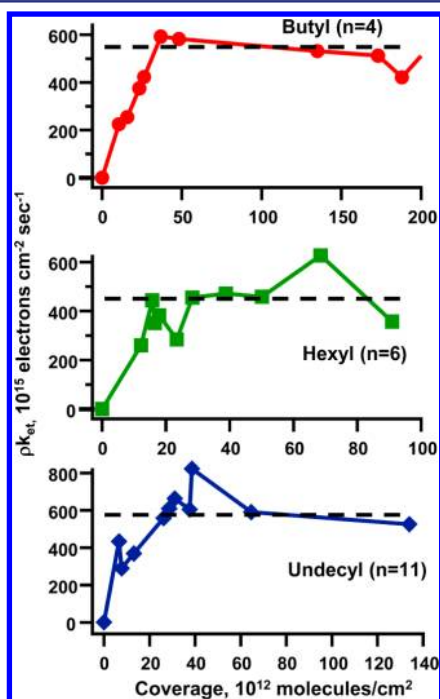
Figure 11. Electron transfer rate per unit area vs surface coverage. The dashed lines are intended only to guide the eye.

The data show that for all three molecules, the total electron-transfer rate (per unit area) increases and then reaches a broader plateau, as the increase in the number of molecules per unit area compensates for the decreased electron transfer rate per molecule. In each case, the data show that the total electron transfer rate plateaus at $\sim(450-600) \times 10^{12}$ electrons cm^{-2} s^{-1}, or $70-100$ $\mu A/cm^2$ limiting rate.

CONCLUSIONS

Our experimental results and molecular dynamics calculations demonstrate that, for the molecular layers studied here, dynamic molecular disorder plays a crucial role in enabling facile electron transfer. The results show that electron transfer within these conformationally disordered monolayers is best described via a through-space (or, more correctly, through-water) tunneling mechanism, in which the relevant distance for electron transfer is controlled by the transient motions of the molecules. Our results show that there is a trade-off between high surface coverage and fast electron transfer rates, but these factors largely compensate for one another so that there is a range of coverages over which the total electron transfer rate per unit area remains nearly constant. Furthermore, longer chains have greater flexibility, such that there is no detectable penalty for increasing the chain length from 4 carbon atoms to 11 carbon atoms. Somewhat contrary to expectations, our results suggest that the best monolayers for applications such as electrocatalytic interfaces are not perfect, well-ordered layers but are in fact, conformationally disordered layers. Disorder is beneficial and, indeed, may even be necessary when using saturated alkyl tethers to integrate redox-active molecules with

covalently bonded materials such as diamond, silicon, and TiO_2. The attachment chemistry we have developed for diamond electrodes shows both high stability and fast electron transfer kinetics and is a promising platform for electron transfer and electrocatalysis.

ASSOCIATED CONTENT

S Supporting Information

Coverage-dependent values of the half-wave potential $E_{1/2}$. Calculated coverage for random bonding of adsorbates onto covalent lattice with fixed bonding points. Videos depicting dynamic motion of diamond-tethered ferrocene groups. This material is available free of charge via the Internet at http://pubs.acs.org.

AUTHOR INFORMATION

Corresponding Author
rjhamers@wisc.edu
Present Address
‡R.E.R.: Dept. of Chemistry, Oregon State University, Corvallis, OR.
Notes
The authors declare no competing financial interest.

ACKNOWLEDGMENTS

REFERENCES

(1) Yao, S. A.; Ruther, R. E.; Zhang, L.; Franking, R. A.; Hamers, R. J.; Berry, J. F. *J. Am. Chem. Soc.* **2012**, *134*, 15632−15635.
(2) Vannucci, A. K.; Chen, Z. F.; Concepcion, J. J.; Meyer, T. J. *ACS Catal.* **2012**, *2*, 716−719.
(3) Ashford, D. L.; Song, W. J.; Concepcion, J. J.; Glasson, C. R. K.; Brennaman, M. K.; Norris, M. R.; Fang, Z.; Templeton, J. L.; Meyer, T. J. *J. Am. Chem. Soc.* **2012**, *134*, 19189−19198.
(4) Glasson, C. R. K.; Song, W. J.; Ashford, D. L.; Vannucci, A.; Chen, Z. F.; Concepcion, J. J.; Holland, P. L.; Meyer, T. J. *Inorg. Chem.* **2012**, *51*, 8637−8639.
(5) Heller, A. *J. Phys. Chem.* **1992**, *96*, 3579−3587.
(6) Albert, K. J.; Lewis, N. S.; Schauer, C. L.; Sotzing, G. A.; Stitzel, S. E.; Vaid, T. P.; Walt, D. R. *Chem. Rev.* **2000**, *100*, 2595−2626.
(7) Lindsey, J. S.; Bocian, D. F. *Acc. Chem. Res.* **2011**, *44*, 638−650.
(8) Aswal, D. K.; Lenfant, S.; Guerin, D.; Yakhmi, J. V.; Vuillaume, D. *Anal. Chem. Acta* **2006**, *568*, 84−108.
(9) Robinson, D. B.; Chidsey, C. E. D. *J. Phys. Chem. B* **2002**, *106*, 10706−10713.
(10) Eckermann, A. L.; Feld, D. J.; Shaw, J. A.; Meade, T. J. *Coord. Chem. Rev.* **2010**, *254*, 1769−1802.
(11) Chidsey, C. E. D. *Science* **1991**, *251*, 919−922.
(12) Chidsey, C. E. D.; Bertozzi, C. R.; Putvinski, T. M.; Mujsce, A. M. *J. Am. Chem. Soc.* **1990**, *112*, 4301−4306.
(13) Collman, J. P.; Devaraj, N. K.; Eberspacher, T. P. A.; Chidsey, C. E. D. *Langmuir* **2006**, *22*, 2457−2464.
(14) Creager, S. E.; Weber, K. *Langmuir* **1993**, *9*, 844−850.
(15) Creager, S. E.; Wooster, T. T. *Anal. Chem.* **1998**, *70*, 4257−4263.
(16) Finklea, H. O. *Electroanal. Chem.* **1996**, *19*, 109−335.
(17) Finklea, H. O.; Hanshew, D. D. *J. Am. Chem. Soc.* **1992**, *114*, 3173−3181.
(18) Finklea, H. O.; Liu, L.; Ravenscroft, M. S.; Punturi, S. *J. Phys. Chem.* **1996**, *100*, 18852−18858.

(19) Finklea, H. O.; Ravenscroft, M. S.; Snider, D. A. *Langmuir* **1993**, *9*, 223−227.

(20) Nahir, T. M.; Bowden, E. F. *J. Electroanal. Chem.* **1996**, *410*, 9−13.

(21) Nahir, T. M.; Bowden, E. F. *Langmuir* **2002**, *18*, 5283−5286.

(22) Porter, M. D.; Bright, T. B.; Allara, D. L.; Chidsey, C. E. D. *J. Am. Chem. Soc.* **1987**, *109*, 3559−3568.

(23) Ravenscroft, M. S.; Finklea, H. O. *J. Phys. Chem.* **1994**, *98*, 3843−3850.

(24) Rowe, G. K.; Carter, M. T.; Richardson, J. N.; Murray, R. W. *Langmuir* **1995**, *11*, 1797−1806.

(25) Creager, S.; Yu, C. J.; Bamdad, C.; O'Connor, S.; MacLean, T.; Lam, E.; Chong, Y.; Olsen, G. T.; Luo, J. Y.; Gozin, M.; Kayyem, J. F. *J. Am. Chem. Soc.* **1999**, *121*, 1059−1064.

(26) Smalley, J. F.; Feldberg, S. W.; Chidsey, C. E. D.; Linford, M. R.; Newton, M. D.; Liu, Y. P. *J. Phys. Chem.* **1995**, *99*, 13141−13149.

(27) Marcinko, S.; Fadeev, A. Y. *Langmuir* **2004**, *20*, 2270−2273.

(28) Liu, Z. M.; Yasseri, A. A.; Lindsey, J. S.; Bocian, D. F. *Science* **2003**, *302*, 1543−1545.

(29) Benson, M. C.; Ruther, R. E.; Gerken, J. B.; Rigsby, M. L.; Bishop, L. M.; Tan, Y. Z.; Stahl, S. S.; Hamers, R. J. *ACS Appl. Mater. Interfaces* **2011**, *3*, 3110−3119.

(30) Martin, H. B.; Argoitia, A.; Landau, U.; Anderson, A. B.; Angus, J. C. *J. Electrochem. Soc.* **1996**, *143*, L133−L136.

(31) Granger, M. C.; Witek, M.; Xu, J. S.; Wang, J.; Hupert, M.; Hanks, A.; Koppang, M. D.; Butler, J. E.; Lucazeau, G.; Mermoux, M.; Strojek, J. W.; Swain, G. M. *Anal. Chem.* **2000**, *72*, 3793−3804.

(32) Hupert, M.; Muck, A.; Wang, R.; Stotter, J.; Cvackova, Z.; Haymond, S.; Show, Y.; Swain, G. M. *Diamond Relat. Mater.* **2003**, *12*, 1940−1949.

(33) Swain, G. M. *J. Electrochem. Soc.* **1994**, *141*, 3382−3393.

(34) Swain, G. M. *Electrically Conducting Diamond Thin Films: Advanced Electrode Materials for Electrochemical Technologies*; Marcel Dekker: New York, 2004; Vol. 22.

(35) Swain, G. M.; Ramesham, R. *Anal. Chem.* **1993**, *65*, 345−351.

(36) Xu, J. S.; Granger, M. C.; Chen, Q. Y.; Strojek, J. W.; Lister, T. E.; Swain, G. M. *Anal. Chem.* **1997**, *69*, A591−A597.

(37) Das, M. R.; Wang, M.; Szunerits, S.; Gengembre, L.; Boukherroub, R. *Chem. Commun.* **2009**, 2753−2755.

(38) Ruther, R. E.; Rigsby, M. L.; Gerken, J. B.; Hogendoorn, S. R.; Landis, E. C.; Stahl, S. S.; Hamers, R. J. *J. Am. Chem. Soc.* **2011**, *133*, 5692−5694.

(39) Devaraj, N. K.; Decreau, R. A.; Ebina, W.; Collman, J. P.; Chidsey, C. E. D. *J. Phys. Chem. B* **2006**, *110*, 15955−15962.

(40) Smalley, J. F.; Finklea, H. O.; Chidsey, C. E. D.; Linford, M. R.; Creager, S. E.; Ferraris, J. P.; Chalfant, K.; Zawodzinsk, T.; Feldberg, S. W.; Newton, M. D. *J. Am. Chem. Soc.* **2003**, *125*, 2004−2013.

(41) Sumner, J. J.; Creager, S. E. *J. Phys. Chem. B* **2001**, *105*, 8739−8745.

(42) Sumner, J. J.; Weber, K. S.; Hockett, L. A.; Creager, S. E. *J. Phys. Chem. B* **2000**, *104*, 7449−7454.

(43) Weber, K.; Hockett, L.; Creager, S. *J. Phys. Chem. B* **1997**, *101*, 8286−8291.

(44) Liu, G. Z.; Liu, J. Q.; Bocking, T.; Eggers, P. K.; Gooding, J. J. *Chem. Phys.* **2005**, *319*, 136−146.

(45) Umana, M.; Rolison, D. R.; Nowak, R.; Daum, P.; Murray, R. W. *Surf. Sci.* **1980**, *101*, 295−309.

(46) Marrani, A. G.; Dalchiele, E. A.; Zanoni, R.; Decker, F.; Cattaruzza, F.; Bonifazi, D.; Pratoc, M. *Electrochim. Acta* **2008**, *53*, 3903−3909.

(47) Evrard, D.; Lambert, F.; Policar, C.; Balland, V.; Limoges, B. *Chem.—Eur. J.* **2008**, *14*, 9286−9291.

(48) Landis, E. C.; Hamers, R. J. *J. Phys. Chem. C* **2008**, *112*, 16910−16918.

(49) Roth, K. M.; Yasseri, A. A.; Liu, Z. M.; Dabke, R. B.; Malinovskii, V.; Schweikart, K. H.; Yu, L. H.; Tiznado, H.; Zaera, F.; Lindsey, J. S.; Kuhr, W. G.; Bocian, D. F. *J. Am. Chem. Soc.* **2003**, *125*, 505−517.

(50) Dalchiele, E. A.; Aurora, A.; Bernardini, G.; Cattaruzza, F.; Flamini, A.; Pallavicini, P.; Zanoni, R.; Decker, F. *J. Electroanal. Chem.* **2005**, *579*, 133−142.

(51) Li, C. Q.; Ren, B. Y.; Zhang, Y.; Cheng, Z. Y.; Liu, X. X.; Tong, Z. *Langmuir* **2008**, *24*, 12911−12918.

(52) Riveros, G.; Meneses, S.; Escobar, S.; Garin, C.; Chornik, B. *J. Chilean Chem. Soc.* **2010**, *55*, 61−66.

(53) Riveros, G.; Garin, C.; Meneses, S.; Escobar, S. *Mol. Cryst. Liq. Crys.* **2010**, *521*, 187−194.

(54) Hauquier, F.; Ghilane, J.; Fabre, B.; Hapiot, P. *J. Am. Chem. Soc.* **2008**, *130*, 2748−2749.

(55) Sachs, S. B.; Dudek, S. P.; Hsung, R. P.; Sita, L. R.; Smalley, J. F.; Newton, M. D.; Feldberg, S. W.; Chidsey, C. E. D. *J. Am. Chem. Soc.* **1997**, *119*, 10563−10564.

(56) Roth, K. M.; Gryko, D. T.; Clausen, C.; Li, J. Z.; Lindsey, J. S.; Kuhr, W. G.; Bocian, D. F. *J. Phys. Chem. B* **2002**, *106*, 8639−8648.

(57) Leung, T. Y. B.; Gerstenberg, M. C.; Lavrich, D. J.; Scoles, G.; Schreiber, F.; Poirier, G. E. *Langmuir* **2000**, *16*, 549−561.

(58) Chidsey, C. E. D.; Loiacono, D. N. *Langmuir* **1990**, *6*, 682−691.

(59) Nuzzo, R. G.; Dubois, L. H.; Allara, D. L. *J. Am. Chem. Soc.* **1990**, *112*, 558−569.

(60) Chidsey, C. E. D.; Liu, G. Y.; Rowntree, P.; Scoles, G. *J. Chem. Phys.* **1989**, *91*, 4421−4423.

(61) Thoms, B. D.; Owens, M. S.; Butler, J. E.; Spiro, C. *Appl. Phys. Lett.* **1994**, *65*, 2957−2959.

(62) Shirley, D. A. *Phys. Rev. B* **1972**, *5*, 4709.

(63) MacKerell, A. D.; Bashford, D.; Bellott, M.; Dunbrack, R. L.; Evanseck, J. D.; Field, M. J.; Fischer, S.; Gao, J.; Guo, H.; Ha, S.; Joseph-McCarthy, D.; Kuchnir, L.; Kuczera, K.; Lau, F. T. K.; Mattos, C.; Michnick, S.; Ngo, T.; Nguyen, D. T.; Prodhom, B.; Reiher, W. E.; Roux, B.; Schlenkrich, M.; Smith, J. C.; Stote, R.; Straub, J.; Watanabe, M.; Wiorkiewicz-Kuczera, J.; Yin, D.; Karplus, M. *J. Phys. Chem. B* **1998**, *102*, 3586−3616.

(64) Brooks, B. R.; Brooks, C. L.; Mackerell, A. D.; Nilsson, L.; Petrella, R. J.; Roux, B.; Won, Y.; Archontis, G.; Bartels, C.; Boresch, S.; Caflisch, A.; Caves, L.; Cui, Q.; Dinner, A. R.; Feig, M.; Fischer, S.; Gao, J.; Hodoscek, M.; Im, W.; Kuczera, K.; Lazaridis, T.; Ma, J.; Ovchinnikov, V.; Paci, E.; Pastor, R. W.; Post, C. B.; Pu, J. Z.; Schaefer, M.; Tidor, B.; Venable, R. M.; Woodcock, H. L.; Wu, X.; Yang, W.; York, D. M.; Karplus, M. *J. Comput. Chem.* **2009**, *30*, 1545−1614.

(65) Brooks, C. L., III; Karplus, M.; Pettit, B. M. *Adv. Chem. Phys.* **1988**, *71*.

(66) Feig, M.; Brooks, C. L., III *Curr. Opin. Struct. Biol.* **2004**, *14*, 217−224.

(67) Ryckaert, J. P.; Ciccotti, G.; Berendsen, H. J. C. *J. Comput. Phys.* **1977**, *23*, 327−341.

(68) Humphrey, W.; Dalke, A.; Schulten, K. *J. Mol. Graphics Modell.* **1996**, *14*, 33−38.

(69) Anariba, F.; DuVall, S. H.; McCreery, R. L. *Anal. Chem.* **2003**, *75*, 3837−3844.

(70) Lang, A. R. *J. Phys. D.: Appl. Phys.* **1993**, *26*, 2239−2244.

(71) Zemek, J.; Potmesil, J.; Vanecek, M.; Lesiak, B.; Jablonski, A. *Appl. Phys. Lett.* **2005**, *87*, 262114.

(72) Visscher, W. M.; Bolsterl., M. *Nature* **1972**, *239*, 504.

(73) Collman, J. P.; Devaraj, N. K.; Chidsey, C. E. D. *Langmuir* **2004**, *20*, 1051−1053.

(74) Devadoss, A.; Chidsey, C. E. D. *J. Am. Chem. Soc.* **2007**, *129*, 53705371.

(75) Gagne, R. R.; Koval, C. A.; Lisensky, G. C. *Inorg. Chem.* **1980**, *19*, 2854−2855.

(76) Ganesh, V.; Sudhir, V. S.; Kundu, T.; Chandrasekaran, S. *Chem. Asian J.* **2011**, *6*, 2670−2694.

(77) McCrory, C. C. L.; Devadoss, A.; Ottenwaelder, X.; Lowe, R. D.; Stack, T. D. P.; Chidsey, C. E. D. *J. Am. Chem. Soc.* **2011**, *133*, 3696−3699.

(78) Rowe, G. K.; Creager, S. E. *Langmuir* **1991**, *7*, 2307−2312.

(79) Laviron, E. *J. Electroanal. Chem.* **1974**, *52*, 355−393.

(80) Laviron, E. *J. Electroanal. Chem.* **1979**, *105*, 35−42.

(81) MacDonald, J. R. *Impedance Spectroscopy. Emphasizing Solid Materials and Systems*; Wiley-Interscience: New York, 1987.

(82) Katz, E.; Lioubashevsky, O.; Willner, I. *J. Am. Chem. Soc.* **2004**, *126*, 15520−15532.

(83) Cole, K. S.; Cole, R. H. *J. Chem. Phys.* **1941**, *9*, 341−351.

(84) Cole, K. S.; Cole, R. H. *J. Chem. Phys.* **1941**, *9*, 341−351.

(85) Wang, Q.; Zhi, F. P.; Wang, W. T.; Xia, X. H.; Liu, X. H.; Meng, F. F.; Song, Y. Y.; Yang, C.; Lu, X. Q. *J. Phys. Chem. C* **2009**, *113*, 9359−9367.

(86) Hurt, R. L.; Macdonald, J. R. *Solid State Ionics* **1986**, *20*, 111−124.

(87) Rowe, G. K.; Creager, S. E. *J. Phys. Chem.* **1994**, *98*, 5500−5507.

(88) Brug, G. J.; Vandeneeden, A. L. G.; Sluytersrehbach, M.; Sluyters, J. H. *J. Electroanal. Chem.* **1984**, *176*, 275−295.

(89) Pajkossy, T. *J. Electroanal. Chem.* **1994**, *364*, 111−125.

(90) Hamann, C. H.; Hamnett, A.; Vielstich, W. *Electrochemistry*; Wiley: Weinheim, 1998.

(91) Hockett, L. A.; Creager, S. E. *Langmuir* **1995**, *11*, 2318−2321.

(92) Forster, R. J.; Faulkner, L. R. *J. Am. Chem. Soc.* **1994**, *116*, 5444−5452.

(93) Ponce, A.; Gray, H. B.; Winkler, J. R. *J. Am. Chem. Soc.* **2000**, *122*, 8187−8191.

(94) Miller, N. E.; Wander, M. C.; Cave, R. J. *J. Phys. Chem. A* **1999**, *103*, 1084−1093.

(95) Brevnov, D. A.; Finklea, H. O.; Van Ryswyk, H. *J. Electroanal. Chem.* **2001**, *500*, 100−107.

(96) Dubois, L. H.; Nuzzo, R. G. *Annu. Rev. Phys. Chem.* **1992**, *43*, 437−463.

(97) Tender, L.; Carter, M. T.; Murray, R. W. *Anal. Chem.* **1994**, *66*, 3173−3181.

(98) Ulgut, B.; Abruna, H. D. *Chem. Rev.* **2008**, *108*, 2721−2736.

(99) Finklea, H. O.; Avery, S.; Lynch, M.; Furtsch, T. *Langmuir* **1987**, *3*, 409−413.

(100) Jiao, J.; Nordfund, E.; Lindsey, J. S.; Bocian, D. F. *J. Phys. Chem. C* **2008**, *112*, 6173−6180.

(101) Valincius, G.; Niaura, G.; Kazakevičienė, B.; Talaikytė, Z.; Kažemėkaitė, M.; Butkus, E.; Razumas, V. *Langmuir* **2004**, *20*, 6631−6638.

(102) Wipf, D. O.; Kristensen, E. W.; Deakin, M. R.; Wightman, R. M. *Anal. Chem.* **1988**, *60*, 306−310.

(103) Haymond, S.; Babcock, G. T.; Swain, G. M. *Electroanalysis* **2003**, *15*, 249−253.

(104) Goss, J. P.; Eyre, R. J.; Briddon, P. R. *Phys. Stat. Solidi B* **2008**, *245*, 1679−1700.

(105) Duan, L.; Bozoglian, F.; Mandal, S.; Stewart, B.; Privalov, T.; Llobet, A.; Sun, L. *Nat. Chem.* **2012**, *4*, 418−423.

(106) Yin, Q.; Tan, J. M.; Besson, C.; Geletii, Y. V.; Musaev, D. G.; Kuznetsov, A. E.; Luo, Z.; Hardcastle, K. I.; Hill, C. L. *Science* **2010**, *328*, 342−345.

(107) Geletii, Y. V.; Botar, B.; Koegerler, P.; Hillesheim, D. A.; Musaev, D. G.; Hill, C. L. *Angew. Chem., Int. Ed.* **2008**, *47*, 3896−3899.

(108) Laitar, D. S.; Muller, P.; Sadighi, J. P. *J. Am. Chem. Soc.* **2005**, *127*, 17196−17197.